IET Circuits, Devices & Systems

Special Issue: Graphene Electronics: Part 2

Journals
The Institution of Engineering and Technology

Graphene oxide thin films for resistive memory switches

ISSN 1751-858X
Received on 19th May 2015
Revised on 10th July 2015
Accepted on 20th July 2015
doi: 10.1049/iet-cds.2015.0170
www.ietdl.org

Indrani Banerjee[1] ✉, Paul Harris[2], Ali Salimian[2], Asim K. Ray[2]

[1]*Department of Physics, Birla Institute of Technology, Mesra, Ranchi 835215, India*
[2]*Institute of Materials and Manufacturing, Brunel University London, Uxbridge, Middlesex UB8 3PH, UK*
✉ *E-mail: indranibanerjee@bitmesra.ac.in*

Abstract: The presence of voltage controlled negative differential resistance was observed in conduction characteristics recorded at room temperature for 300 nm thick spin-coated films of graphene oxide (GO) sandwiched between indium tin oxide (ITO) substrates and top electrodes of sputtered gold (Au) film. The GO crystallites were found from the X-ray diffraction studies to have an average size in the order of 7.24 nm and to be preferentially oriented along (001) plane. Raman spectroscopy suggested that the material consisted of multilayer stacks with the defects being located at the edges with an average distance of 1.04 nm apart. UV visible spectroscopy studies suggested that the band gap of the material was 4.3 eV, corresponding to direct transitions. The two-terminal ITO/GO/Au devices exhibited memristor characteristics with scan-rate dependent hysteresis, threshold voltage and On/Off ratios. A value of $>10^4$ was obtained for On/Off ratio at a scan rate of 400 mVs^{-1} and 4.2 V.

1 Introduction

In this age of digitally stored information, the demand for high-density, low-power, high-speed, rapidly programmable memory devices is enormous. There are a large number of applications for such devices, for example, in military, industrial and emerging consumer electronics industries, including mobile phones, toys, cards, badges, value paper, medical disposables and so on [1, 2]. Memories may be classified broadly into two categories: volatile and non-volatile (NVM) devices. Static random access memories (SRAM) and dynamic RAM (DRAM) are fast but volatile, thereby increasing the energy cost and requiring additional peripheral circuitry. NVM memories, which retain information when the power is switched off, are capable of undergoing an ideally unlimited number of read/write voltage cycles. NVM silicon-based floating gate flash memory devices are currently dominating mass storage market but suffer from poor endurance, slow read/write speeds and high voltage requirements for write operations. Stress-induced leakage currents limit the oxide thickness to 10 nm, affecting the retention of data [3]. However, silicon nanocrystals have recently been employed for effective charge storage in the low cost fabrication of scaled down non-volatile flash memory with fast erase time and source-side injection programme time both in the order of a few µS [4]. Ferroelectric random access memories (FRAM) utilise the existence of two electric field dependent distinguishable polarisation states and are widely used in the integrated circuits involving smart cards and wireless tags that consume low power for high speed operation with good cyclability. The comparable FRAM density may be achieved with 3D capacitors of an increased area [5]. In a conventional magnetoresistive random access memory (MRAM), the tunnel junction memory cell is switched between magnetic off and on states produced by electrical current. By careful control of the spin polarised current with a view to switching between two suitable magnetisation states, spin transfer torque MRAMs exhibit long endured, comparable performance in terms of capacity, read/write speed and non-volatility of DRAMs, SRAMS and Flash, respectively [6].

There has been growing interest in non-volatile resistance-switching random access memory (RRAM) due to its high operation speed, high scalability, and multi-bit storage potential. RRAM devices consist of a insulating switching layer sandwiched between two metal electrodes (MIM) and are non-destructively operated between high resistance states (HRS) and low resistance states (LRS) through electrical stimulus [7]. Switching and voltage-controlled negative resistance phenomena are reported to have been observed in a large variety of solid-state insulating and semi-conductor materials such as GeSe and Ag_2S, perovskites such as $SrZrO_3$, $Pr_{0.7}Ca_{0.3}MnO_3$, and $BiFeO_3$, binary transition metal oxides such as NiO, TiO_2, ZrO_2, and ZnO, amorphous silicon and solid electrolytes [8–12]. NVM resistive switches have significantly been scaled down in recent years using silicon nano-crystals and metallic nanoparticles [13]. Organic flexible memories can be very economically fabricated on at room temperature on both solid and flexible substrates, using a roll-to-roll large area manufacturing method [14, 15].

Carbon-based materials such as graphene oxide (GO) have been identified as a promising non-volatile memory technology for large area flexible applications [16]. GO sheets consist of hexagonal rings based on networks having both sp^2 and sp^3 hybridised carbon atoms and also carbon bearing hydroxyl and epoxide groups that act as oxygen containing defects and enable it to be easily dispersed in water. Carboxyl and carbonyl groups at sheet edges also make the material more easily dispersible and hence the processing of GO films over large area of solid and flexible substrates for designing RRAM. [17]. It is recently reported that spin-coated GO films in the sandwich configuration between the indium tin oxide (ITO) substrate and evaporated silver electrode exhibit stable performance with high on/off ratio at room temperature under relatively low programming voltage. However deterioration of this performance is found to occur with the rise in temperature possibly due to the change in charge distribution in the GO film and charge injection from the Ag electrode with temperature [18]. Reduction in power by a factor of 10^3 is estimated for tuneable tunnelling barrier in vertical heterostructures of graphene and titanium oxide [19]. A key advantage of this material is the ease with which it is possible to fabricate devices from it using room temperature spin-coating processes and the results of Van Der Pauw measurements for dc conductivity on spin-coated GO samples have recently been reported by us [20].

This paper presents a non-volatile memory device based on GO thin films sandwiched between a sputtered gold top electrode and ITO substrate. The applied field-assisted migration of oxygen

This is an open access article published by the IET under the Creative Commons Attribution License
(http://creativecommons.org/licenses/by/3.0/)

functional groups such as epoxide, hydroxyl and carboxyl groups from the GO edge near the top electrode into the bulk is believed to be responsible for the transition from HRS to LRS states due to accumulation of additional π-electrons in dominant sp^2 bonds [21]. To investigate the physical nature of this resistive mechanism, measurements of the current-voltage characteristics have been performed on ITO/GO/Au as the bias voltage is swept in both forward and reverse directions between ±5 V through 0 V for different scan rates varying from 5 to 400 mVs^{-1}. The degrees of hysteresis in the current-voltage characteristics, threshold voltage and on/off ratio are found to be dependent upon the scan rate. These experimental results have been interpreted in terms of a circuit model to explain the voltage controlled differential negative resistance behaviour. This observation is similar to the effect recently reported for the two terminal Au/ZnO/ITO sandwich devices during the voltage cycling at scan rates ranging from 10 to 500 mVs^{-1} [22].

2 Experimental

Thin films of GO were deposited by spin-coating onto an ultrasonically cleaned suitable substrate depending upon the type of measurement. A 40 weight% dispersion of GO nanoparticles in water (supplied by Sigma-Aldrich) was spin-coated at 850 and 2500 rpm in a sequence for 15 s and 60 s respectively at room temperature. The aqueous solvent was then completely removed by oven drying at 100°C in air. The spin-coated samples were examined using a Zeiss Supra 35VP field emission scanning electron microscope (FESEM). A 10 keV beam was used in conjunction with an in-lens secondary electron detector system. The X-ray diffraction (XRD) pattern of the drop cast GO film on a glass substrate was recorded using Bruker D8 Advance instrument scanning in the 2θ range of 5–100°, with a step size of 0.02° p/s using Cu$K\alpha$ radiation of wavelength 0.15406 nm. Raman spectroscopic studies were carried out on the spin-coated sample using a Horiba Jobin–Yvon LabRAM HR800 instrument fitted with an argon laser (514 nm). UV-visible absorption spectra of spin-coated GO on quartz substrates were recorded using a Perkin–Elmer LAMBDA 650 spectrophotometer between 400 to 800 nm scanning at the rate 654.8 nm/min. The architecture of GO based two terminal device was a simple sandwich structure between the ITO substrate and sputtered gold electrode as shown in Fig. 1*a*. The current (I) passing through the device was measured using a Keithley 617 electrometer in a microprocessor controlled system as the bias voltage (V) was cycled between ±5 V at scan rates ranging from 5 to 500 mV/s with the ITO electrode grounded. The connecting leads were calibrated for low current measurements.

3 Results and discussions

The results of studies of morphology, structure and the vibrational studies on GO films have been presented. The electrical characteristics of the Au/GO/ITO device have also been analysed.

3.1 GO thin film characterisation

Fig. 1*b* shows a FESEM micrograph of the spin-cast GO film. Densely packed, compact formed into widely spread sheets of GO nanocrystals having large surface area are visible. The morphology resembles strongly folded sheets of GO. This indicates that the sheets are mostly overlapped and folded rather than agglomerated.

Fig. 2*a* shows the XRD spectrum for the drop-cast GO sample. Drop-cast GO films were used for this investigation to apply

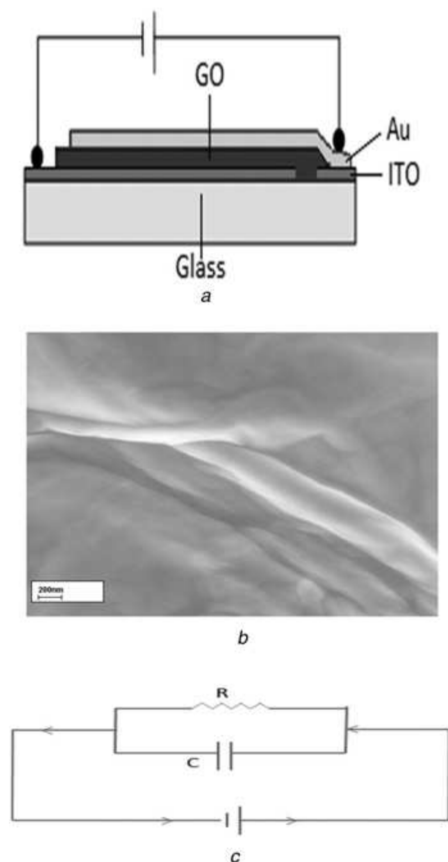

Fig. 1 *Architecture of GO based two terminal device was a simple sandwich structure between the ITO substrate and sputtered gold electrode*

a Sandwich structure of the GO between the ITO and gold electrode
b SEM image of GO film and
c equivalent circuit for the device in Fig. 1*a*

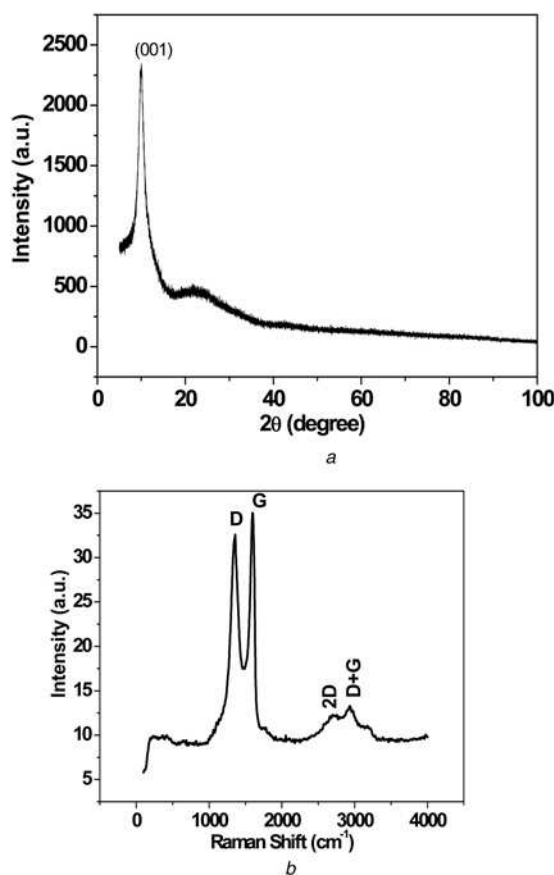

Fig. 2 *XRD and Raman spectra*

a XRD pattern of a drop-cast GO sample on a glass substrate
b Raman spectrum of GO film spin-coated onto an ITO glass substrate

This is an open access article published by the IET under the Creative Commons Attribution License (http://creativecommons.org/licenses/by/3.0/)

thicker coatings so as to improve the signal to noise ratio, which was poor for the thin spin-coated samples. The sharp diffraction peak at $2\theta = 10°$ is identified with the (001) plane of GO. The position of the Bragg peak is susceptible to the extent of oxidation and ambient environment [23, 24]. The interlayer distance (*d*-spacing) is estimated to be 0.88 nm from Bragg's law. The interlayer distance is larger than the reported value of 0.335 nm for pristine graphite corresponding to a diffraction peak at 27°. This increase in the *d*-spacing may be attributed to the possible presence of oxygen containing functional groups on the GO edge [25]. Using the Scherrer equation, the mean crystalline diameter and the average number of layers in a crystallite were found to be 7.24 nm and ~8 respectively. These values are in agreement with those obtained for sonochemically synthesised GO films, implying an improvement of film quality over one formulated by the conventional method [26].

The Raman spectrum in Fig. 2*b* of the GO spin-coated film shows four peaks at 1350, 1580, 2680 and 2950cm^{-1} which are identified as *D*, *G*, 2D and $D+G$ bands, respectively. The *D* peak represents the breathing mode of aromatic rings arising due to the defects in the sample and therefore its peak intensity is often used as a measure of the degree of disorder. The *G* peak corresponds to the optical E_{2g} phonons at the Brillouin zone centre resulting from the bond stretching of sp^2 carbon pairs in rings and chains both. The ratio of I_D/I_G is reported to be increase as the defects become further apart, to a maximum of ~3 at a spacing of 3.2 nm and thereafter decreases. The I_D/I_G ratio and FWHM of these peaks provide quantitative information regarding the distance L_D between defects as a measure of the amount of disorder. It has been reported that the intensity ratio between 0 and 3.5 exhibit a skewed parabolic dependence on L_D in the range of 1 to 10 nm, reaching the peak of ~3 at $L_D = 3.2$ nm. Using this characteristic behaviour, the ratio $I_D/I_G = 0.938$ corresponds to $L_D = 1.04$ nm for values of 136 and 69 cm^{-1} obtained in this work for FWHM for *D* and *G* bands respectively [26]. These defects are likely to be predominantly at the edges of the flakes [27]. The relatively weak 2D peak is attributed to double resonance transitions resulting in the production of two phonons with opposite momentum. The 2D band for monolayer graphene is sharp and symmetric about the centre; a broad band seen for the sample under the present investigation indicates of multiple-layer stacking. The intensity ratio of I_G/I_{2D} for the sample was found to be ~2.8 implying the presence of both single and multiple layers. $D+G$ peak at 2950 cm^{-1} also indicates the disorder on GO and the presence of defects [28].

Fig. 3*a* displays the UV-visible spectrum of the GO film on a quartz substrate. The absorption peak is observed at 230 nm which is attributed to π-π* transition of the atomic C-C bonds and the shoulder peak at ~ 300 nm corresponds to *n*-π* transitions of aromatic C-C bonds [29]. The Tauc plot of $(Ah\nu)^2$ against incident photon energy hν in Fig. 3*b* is found to be linear over the range of photon energies from 4.5 to 5 eV, where A is the measured absorbance. This linear dependence above the fundamental absorption edge implies the existence of direct transitions [30]. The magnitude of the band gap was found to be 4.3 eV from extrapolation of this linear portion to the intercept of the ordinate corresponding to $A = 0$. These indirect wideband features are in good agreement with reported observation on GO films synthesised by a modified Hummers'procedure [31]. The width of the localised states tailing into the band gap was estimated to be 1.3 eV from the Urbach plot of ln(A) versus (hν) shown in Fig. 3*c*. The refractive index of 2.1 was calculated from the Lorentz–Lorenz equation for electronic polarisability in the modified form of $(n^2-1)/(n^2+2) = 1-\sqrt{Eg/20}$ [32].

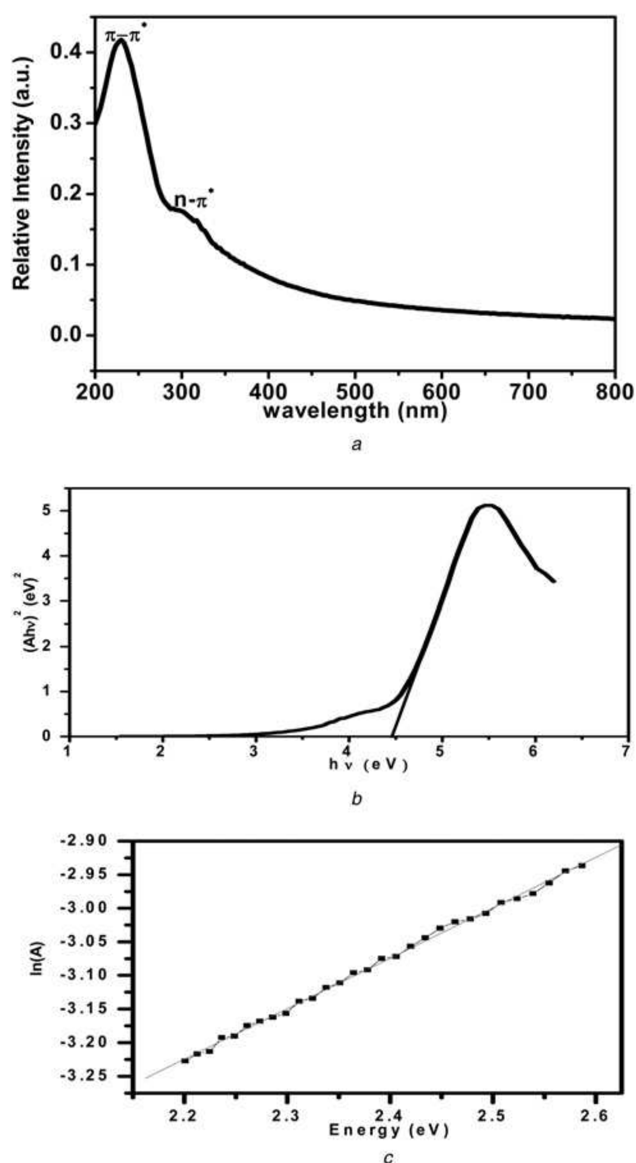

Fig. 3 *Displays the UV-visible spectrum of the GO film on a quartz substrate*

a UV-visible absorbance spectrum of spin-coated GO on a quartz substrate
b Tauc plot of $(Ah\nu)^2$ against incident photon energy hν ($4\text{eV} \le h\nu \le 6$ eV) and
c Urbach plot of ln(A) against hν ($2.2\text{eV} \le h\nu \le 2.6$ eV)

3.2 Electrical measurements

A set of reproducible current-voltage [$I(V)$] characteristics in Fig. 4 was recorded for a single cycle at room temperature for the Au/GO/

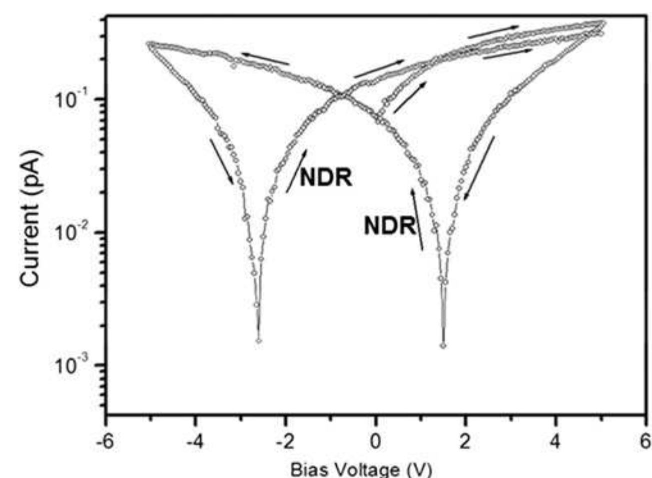

Fig. 4 *Current-voltage [I(V)] characteristics of ITO/GO/Au sample at room temperature for the scan rate of 5 mVs^{-1}, arrows indicating the direction of the sweep*

This is an open access article published by the IET under the Creative Commons Attribution License (http://creativecommons.org/licenses/by/3.0/)

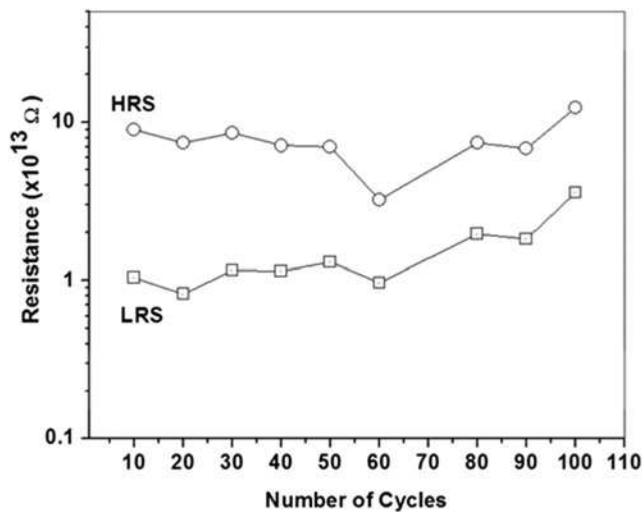

Fig. 5 *High-resistance (closed circles) and low resistance (closed square) over 100 cycles at the bias voltage of 1.5 V and 5 mVs^{-1}*

ITO device as the bias voltage V was swept at the scan rate of 5 mVs^{-1} in both forward and reverse directions between ±5 through 0 V. It is evident that the current level in the first forward sweep from 0 to +5 V (low resistance ON state) is greater than that in the reverse sweep from +5 V. Two types of behaviour are found to exist in the reverse sweep separated by the threshold voltage $V_T^+ = 1.8$ V corresponding to dI/dV = 0. The first type represents the high resistance Off state with continual decrease in current as the bias voltage V is progressively reduced from +5 V until the threshold voltage of 1.8 V. The On–Off ratio which is defined as the ratio of current in the ON state to that in the Off state corresponding to a given bias voltage is found to be 2×10^2 at the threshold voltage $V_T^+ = 1.8$ V. Second, the rise in I is observed with respect to decreasing V in the bias voltage from 1.8 to 0 V, giving rise to the almost symmetrical voltage-controlled negative differential resistance (NDR) effect. The On and Off states were also found to exist as the device was cycled between 0 to −5 V and back to $V_T^- = -2.5$ V at which the NDR regime was found to have set in.

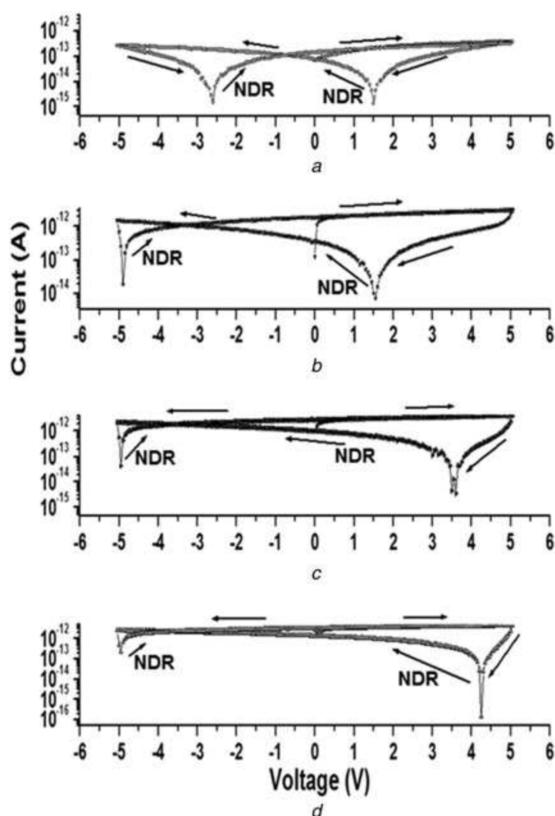

Fig. 6 *Current-voltage [I(V)] characteristics of ITO/GO/Au sample at room temperature for the scan rate of*

a 25 mVs^{-1}
b 50 mVs^{-1}
c 100 mVs^{-1}
d 400 mVs^{-1}

During the LRS state, filamentary conducting channels are believed to have formed by oxygen vacancies and electron traps in the GO matrix connecting two electrodes resulting from the field-assisted migration of oxygen-related functional groups such as epoxide, hydroxyl and carboxyl groups at the GO edge near the top Au electrode into the GO bulk. As a result, the concentration of interlayer π electrons increases as sp^2 bonding becomes dominant over sp^3 bonding, giving rise to high conductance. As the voltage is swept in the reverse direction, the oxygen-related groups diffuse into the GO edge from the ITO electrode giving rise to the LRS regime [33]. The replenishment of oxygen vacancies in the GO film becomes complete at the threshold voltage possibly due to migration of oxygen ions from the ITO substrate and conducting filaments have now been ruptured. For

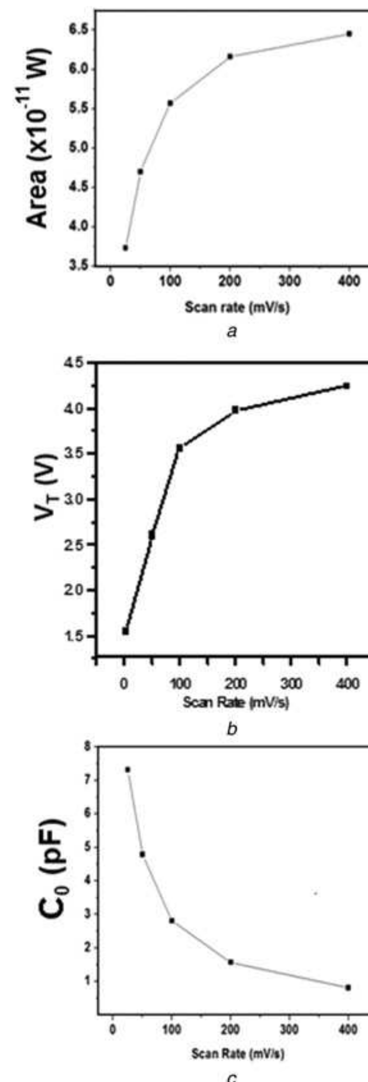

Fig. 7 *Scan-rate dependence*

a Hysteresis area
b Zero bias capacitance C_0
c Threshold voltage V_T

This is an open access article published by the IET under the Creative Commons Attribution License (http://creativecommons.org/licenses/by/3.0/)

further decrease in the bias voltage V, the migration of oxygen-related groups begins to take place with gradual reforming of the GO layer, resulting in NDR. Similar arguments are also applicable for the negative bias regime but functional groups at the GO edge near the ITO electrode become active in this case. The presence of these groups at the GO edges is consistent with our earlier observation from the Raman spectroscopy.

The stability of the device has been examined by performing the measurements over 100 voltage cycles between 0 and 5 V and 5 and 0 V at the scan rate of 5 mV/s. Fig. 5 shows the variation of HRS and LRS recorded in different cycles. For the first 50 cycles, the ratio of HRS to LRS is found to be approximately 10. Further voltage cycling appears to have considerable effect on endurance of the switch as the ratio is reduced to 4. This type of variation is expected because of statistical nature of the formation and rupture of conducting filaments. However, both HRS and LRS remain well resolved and there is no overlapping between two states, indicating the reasonably stable and non-volatile features of the Au/GO/ITO memory resistive switch.

As shown in Fig. 6, the existence of multiple resistive states is also observed when the measurements are repeated for the voltage cycling at four higher scan rates rising to 400 mVs^{-1}. The degree of the hysteresis which shows clearly the transition between HRS and LRS during the voltage sweeps is found to be dependent upon the scan rate $\tau (= dV/dt)$. The effect may be explained in terms of an equivalent circuit in Fig. 1*c* consisting of two passive components, resistance R and capacitance C in parallel is proposed to explain the characteristic features of $[I(V)]$ curves of the Au/GO/ITO device. The net current I is the sum of the displacement components in the form

$$I = \frac{V}{R} + C(V)\tau + V\tau\left(\frac{dC}{dV}\right) \quad (1)$$

This circuit is consistent with charge-trapping mechanisms which are relevant for the present case in light of earlier observation from Raman spectral studies of the presence of the defects and stacking layers in GO thin films. (dC/dV) and $C(V)$ are regarded as being largely responsible for determining the magnitude of the hysteresis. For $dI/dV = 0$, the threshold voltage V_T is obtained in the form

$$V_T = -\frac{(1/R\tau) + 2(dC/dV)}{d^2C/dV^2} \quad (2)$$

Numerically computed values of the hysteresis loop area in Fig. 7*a* displays a sharp rise from 3.75×10^{-11} W to 6.25×10^{-11} W as the scan rate is increased from 5 mV/s to 200 mV/s. This behaviour is followed by slow tendency at higher scan rates for saturation to occur. This implies that the power consumption of the switch is smaller at slow τ than that at fast τ. Similar increase of V_T with respect to the scan rate is observed in Fig. 7*b*, indicating the occurrence of filament rupture at higher voltage for high τ than low τ. Values of zero bias capacitance C_0 are estimated from the knowledge that the short circuit current $I_{sc} = C_0\tau$ corresponding to $V = 0$ using (1). Fig. 7*c* displays a sharp decrease of C_0 with increasing τ. The available response time for charges responsible for filamentary conduction to align with the changing applied field becomes shorter with the increase in the scan rate. At the low voltage scan rate, the charge carriers have sufficiently large relaxation time to respond to the relatively slow voltage variation. On the other hand, charge carriers are too slow to relax to the fast changing voltage.

The on/off ratio of currents in the OFF and ON states are shown in Fig. 8 for different scan rates. The on/off ratio reaches a maximum value at threshold voltage V_T for each scan rate and the highest value of 4×10^4 has been achieved for on/off ratio of the ITO/GO/Au resistive switch corresponding to $V_T^+ = 4.3$ V at the scan rate of 400 mV/s. The present results are at least two orders of magnitude higher than those reported for the switch made of the spin-coated GO film sandwiched between aluminium electrode and the polyethersulfone substrate [34].

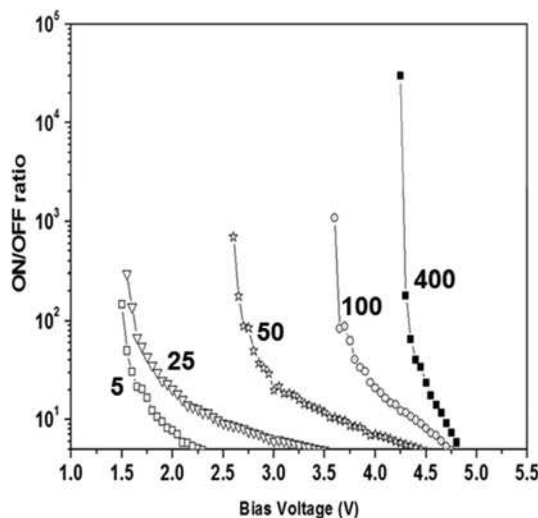

Fig. 8 *Dependence of On–OFF ratio of the ITO/GO/Au switch on the bias voltage for the scan rate of*

a 5 mVs^{-1} (open squares)
b 25 mVs^{-1} (open triangles)
c 50 mVs^{-1} (open stars)
d 100 mVs^{-1} (open circles)
e 400 mVs^{-1} (closed squares)

4 Conclusions

Commercially available GO nanoparticle dispersions have been used in this study to produce spin-coated thin films. It is found that the sequential use of two speeds of 850 and 2500 rpm for 15 and 60 s, respectively is suitable for the cost-effective formulation of high quality, uniform GO film. XRD spectroscopic studies reveal the formation of an eight layered polycrystalline structure preferentially oriented along (001) plane, with average GO crystallite size in the order of 7.24 nm. Defects are situated at the edges of the GO flakes with an average distance between them of about 1.04 nm. The electronic transition was found to be indirect over a wide bandgap of 4.3 eV. The occurrence of NDR is observed in the room temperature $I(V)$ characteristics of the two terminal ITO/GO/Au devices as the bias voltage V is swept in both forward and reverse directions between ±5 through 0 V. The formation and rupture of conducting filaments are believed to be responsible for this type of behaviour. The degree of hysteresis is found to dependent upon the scan rate τ as the rate is varied from 5 to 400 mVs^{-1}. The on/off ratio is found to be increasing with the rise in the scan rate, giving a value of the ratio $\geq 10^4$ at $\tau = 400$ mVs^{-1} corresponding to $V_T = 4.2$ V. An equivalent circuit model predicts increasing power consumption with increasing scan rate τ, implying that an optimum trade-off between power consumption and on/off ratio needs to be identified for a given application.

5 Acknowledgment

Dr Indrani Banerjee is grateful to Commonwealth Association, UK for funding the present research work under the fellowship placement scheme (grant reference INCF-2014-66).

6 References

1 Meena, J.S., Sze, S.M., Chand, U., *et al.*: ‘Overview of emerging nonvolatile memory technologies’, *Nanoscale Res. Lett.*, 2014, **9**, Article Number: 526

This is an open access article published by the IET under the Creative Commons Attribution License (http://creativecommons.org/licenses/by/3.0/)

2 Mikolajick, T., Salinga, M., Kund, M., *et al*.: 'Nonvolatile memory concepts based on resistive switching in inorganic materials', *Adv. Eng. Mater.*, 2009, **11**, (4), pp. 235–240

3 Hoefler, A., Higman, J.M., Harp, T., *et al*.: 'Statistical modeling of the program/erase cycling acceleration of low temperature data retention in floating gate nonvolatile memories'. 40th Annual IEEE Int. Reliability Physics Symp., Dallas, Texas, 7–11 April 2002, pp. 21–25

4 Yater, J.A.: 'Implementation of Si nanocrystals in non-volatile memory devices', *Phys. Status Solidi A-Appl. Mater.*, 2013, **210**, (8), pp. 1505–1511

5 Fujisaki, Y.: 'Review of emerging new solid-state non-volatile memories', *Jpn. J. Appl. Phys.*, 2013, **52**, (4), Article Number: 040001, pp. 1–11

6 Chen, E., Apalkov, D., Driskill-Smith, A., *et al*.: 'Progress and prospects of spin transfer torque random access memory', *IEEE Trans. Magn.*, 2012, **48**, (11), pp. 3025–3030

7 Beck, A., Bednorz, J.G., Gerber, Ch., *et al*.: 'Reproducible switching effect in thin oxide films for memory applications', *Appl. Phys. Lett.*, 2000, **77**, (1), pp. 139–141

8 Jeong, D.S., Thomas, R., Katiyar, R.S., *et al*.: 'Emerging memories: resistive switching mechanisms and current status rep', *Prog. Phys.*, 2012, **75**, (7), Article Number: 076502, pp. 1–31, doi: 10.1088/0034-4885/75/7/076502

9 Li, Y.T., Long, S.B., Liu, Q., *et al*.: 'An overview of resistive random access memory devices', *Chin. Sci. Bull.*, 2011, **56**, (28–29), pp. 3072–3078

10 Dong, Y., Yu, M.G., Mc Alpine, C., *et al*.: 'Si/α-Si core/shell nanowires as nonvolatile crossbar switches', *Nano Lett.*, 2008, **8**, (2), pp. 386–391

11 Lu, W., Lieber, C.M.: 'Nanoelectronics from the bottom up', *Nat. Mater.*, 2007, **6**, (11), pp. 841–850

12 Lee, M.J., Park, Y., Suh, D.S., *et al*.: 'Two series oxide resistors applicable to high speed and high density nonvolatile memory', *Adv. Mater.*, 2007, **19**, (22), pp. 3919–3923

13 Verrelli, E., Tsoukalas, D.: 'Cluster beam synthesis of metal and metal-oxide nanoparticles for emerging memories', *Solid-State Electron.*, 2014, **101**, (SI), pp. 95–105

14 Heremans, P., Gelinck, G.H., Muller, R., *et al*.: 'Polymer and organic nonvolatile memory devices', *Chem. Mater.*, 2011, **23**, (3), pp. 341–358

15 Sleiman, A., Mabrook, M.F., Nejm, R.R., *et al*.: 'Organic bistable devices utilizing carbon nanotubes embedded in poly(methyl methacrylate)', *J. Appl. Phys.*, 2012, **112**, (2), Article Number: 024509, pp. 1–5

16 Liu, J.Q., Yin, Z.Y., Cao, X.H., *et al*.: 'Fabrication of flexible, all-reduced graphene oxide non-volatile memory devices', *Adv. Mater.*, 2013, **25**, (2), pp. 233–238

17 Lin, C.C., Wu, H.Y., Lin, N.C., *et al*.: 'Graphene-oxide-based resistive switching device for flexible nonvolatile memory application', *Jpn. J. Appl. Phys.*, 2014, **53**, (5), Special Issue: 1 Article Number: 05FD03, pp. 1–7

18 Yi, M.D., Cao, Y., Ling, H.F., *et al*.: 'Temperature dependence of resistive switching behaviors in resistive random access memory based on graphene oxide film', *Nanotechnology*, 2014, **25**, (18), pp. 1–7, doi: 10.1088/0957–4484/25/18/185202

19 Qian, M., Pan, Y.M., Liu, F.Y., *et al*.: 'Tunable, ultralow-power switching in memristive devices enabled by a heterogeneous graphene-oxide interface', *Adv. Mater.*, 2014, **26**, (20), pp. 3275–3281

20 Li, T., Patel, T., Banerjee, I., *et al*.: 'Plasma treated graphene oxide films: structural and electrical studies', *J. Mater. Sci. Mater. Electron.*, 2015, **26**, (7), pp. 4810–4815, doi: 10.1007/s10854–015-3122-0

21 He, C.L., Zhuge, F., Zhou, X.F., *et al*.: 'Nonvolatile resistive switching in graphene oxide thin films', *Appl. Phys. Lett.*, 2009, **95**, (23), Article Number: 232101, pp. 1–3, doi: 10.1063/1.3271177

22 Paul, S., Harris, P.G., Pal, C., *et al*.: 'Low cost zinc oxide for memristors with high on-off ratios', *Mater. Lett.*, 2014, **130**, pp. 40–42

23 Jeon, K.W., Seo, D.K.: 'Concomitant thionation and reduction of graphene oxide through solid/gas metathetical sulfidation reactions at high temperatures', *Phosphorus Sulfur Silicon Relat. Elem*, 2014, **189**, (6), pp. 721–737

24 Shin, H.J., Kim, K.K., Benayad, A., *et al*.: 'Efficient reduction of graphite oxide by sodium borohydride and its effect on electrical conductance', *Adv. Funct. Mater.*, 2009, **19**, (12), pp. 1987–1992

25 Zhao, W.W., Kido, G., Harada, S., *et al*.: 'Synthesis and characterization of anisotropically expanded graphite oxide compounds derived from spherical graphite', *J. Colloid Interface Sci.*, 2014, **431**, pp. 8–16

26 Esmaeili, A., Entezari, M.H.: 'Facile and fast synthesis of graphene oxide nanosheets via bath ultrasonic irradiation', *J. Colloid Interface Sci.*, 2014, **432**, pp. 19–25

27 Eigler, S., Dotzer, C., Hirsch, A.: 'Visualization of defect densities in reduced graphene oxide', *Carbon*, 2012, **50**, (10), pp. 3666–3673

28 Yeh, T.F., Syu, J.M., Cheng, C., *et al*.: 'Graphite oxide as a photocatalyst for hydrogen production from water', *Adv. Funct. Mater.*, 2010, **20**, (14), pp. 2255–2262

29 Cancado, L.G., Takai, K., Enoki, T., *et al*.: 'General equation for the determination of the crystallite size L-a of nanographite by Raman spectroscopy', *Appl. Phys. Lett.*, 2006, **88**, (16), Article Number: 163106, pp. 1–3

30 Ray, A.K., Hogarth, C.A.: 'On the analysis of experimental-data for optical-absorption in noncrystalline materials', *J. Phys. D-Appl. Phys.*, 1990, **23**, (4), pp. 458–459

31 Yeh, T.F., Syu, J.M., Cheng, C., *et al*.: 'Graphite oxide as a photocatalyst for hydrogen production from water', *Adv. Funct. Mater.*, 2010, **20**, (14), pp. 2255–2262

32 Dimitrov, V., Sakka, S.: 'Electronic oxide polarizability and optical basicity of simple oxides', *J. Appl. Phys.*, 1996, **79**, (3), pp. 1736–1740

33 Khurana, G., Misra, P., Katiyar, R.S.: 'Forming free resistive switching in graphene oxide thin film for thermally stable nonvolatile memory applications', *J. Appl. Phys.*, 2013, **114**, p. 124508

34 Jeong, H.Y., Kim, J.Y., Kim, J.W., *et al*.: 'Graphene oxide thin films for flexible nonvolatile memory applications', *Nano Lett.*, 2010, **10**, pp. 4381–4386

This is an open access article published by the IET under the Creative Commons Attribution License
(http://creativecommons.org/licenses/by/3.0/)